Model. Earth Syst. Environ. (2015) 1:44
DOI 10.1007/s40808-015-0046-x

ORIGINAL ARTICLE

3D Mechanical modeling of faults planes based on stress fields: a case study of Saravan fault, SE Iran

Pouya Sadeghi[1] · Mohammad Mahdi Khatib[2] · Ali Asghar Moridi[3] · Sasan Bagheri[3]

Received: 4 November 2015 / Accepted: 7 November 2015 / Published online: 21 November 2015

Abstract This research aims to understand the response of the faults planes subjected to the certain stress fields. When an active fault ruptures, its geometry depends to the responsible mechanism at geological time. Therefore, it is important to study the faults behavior based on stress fields. We try to provide a process of modeling the fault plane. We first gain stress field by MATLAB scripting based on field data and stress–strain analyses. In addition, we compare the morphology of analogue models with the study area to improve our model. We design mechanical models based on finite element methods in Ansys so that have more adaptation with stress field and surface deformations. Finally, 3D fault plane appears as a narrow part of solid block. Selecting Saravan fault in SE Iran is because of its significant curvature along its strike and its recent activity. The model represents a compression and bulking affecting to the study area. The 3D deformed fault plane as a part of hanging wall block shows an upward progressive tear zone at the south end of the main fault.

✉ Pouya Sadeghi
pouya.sadeghi@rocketmail.com;
pouya.sadeghi@birjand.ac.ir

Mohammad Mahdi Khatib
mkhatib@birjand.ac.ir

Ali Asghar Moridi
amoridi@science.usb.ac.ir

Sasan Bagheri
sasan@hamoon.usb.ac.ir

[1] Tectonics Laboratory, Department of Geology, University of Birjand, Birjand, Iran

[2] Department of Geology, University of Birjand, Birjand, Iran

[3] Department of Geology, University of Sistan and Baluchestan, Zahedan, Iran

Keywords Stress field · Mechanical model · Finite element method

Introduction

Many items including stress state, crustal geometry, rheology, rock type, frictional resistance, and fault activity interact to form tectonic phenomena (Rowshandel and Nemat-Nasser 1986; Niño et al. 1998; Chéry et al. 2004). Therefore we can use a continuous mechanical process to study the simultaneous effects of many geological events (Niño et al. 1998).

The aim of this study is applying a 3D mechanical model using stress fields to find out the geometry of the faults planes that here is Saravan fault (SF) as a case study. SF is an active right lateral reverse fault in SE Iran. An Mw 7.7 earthquake struck the Saravan region in SE Iran on 16 April 2013. According to the EMSC reports an almost pure normal focal mechanism with NE–SW fault plane, with a focal depth of 84 km (Zare and Shahvar 2013).

Since SF has reverse dip component and normal focal mechanism is unusual, we are interested to consider fault plane if there is another rupture at depth. By having an overall 3D view about fault plane, the judgment about seismic behavior of fault is more possible. We use a 3D finite element model and apply rock mechanical data to get a more realistic model.

Primitive investigators have considered elastic (e.g. Steketee, 1958; Chinnery 1961, 1970; Weertman 1965; Rybicki 1971) and viscoelastic (Nur and Mavko 1974) rheology in mechanical models. Considering of solid characteristics began with frictional resistance of rocks studies for strike slip faults and geodynamical models (Stuart 1979, 1981; Stuart and Mavko 1979; Rowshandel

and Nemat-Nasser 1986; Carlson and Langer 1989; Willet et al. 1993; Byrne et al. 1993; Beaumont et al. 1996). However, the conception of modern mechanical models started with considering deformation fields and stress measurements (Niño et al. 1998; Chéry et al. 2001, 2004; Rhoden et al. 2012).

In this research, we improve mechanical models by taking stress field simulation and affecting rock mechanical data into account. Among main items for modeling, the state of stress is most important. By using MTLAB coding for structural field data, we simulate stress field. In this study, we try to design a mechanical model that works with simulated stress fields. We consider hanging wall block and then select narrow part of it to control boundary condition and study deformations of the fault plane. Therefore, Three-dimension geometry of SF plane due to the responsible mechanics is the focus of this research.

Geological setting

General geology

The study area lies on the Nehbandan–Khash structural zone (Nabavi 1976) in southeastern Iran. However, there are some other names for this zone such as Iran's East Mountain (Alavi 1991), Sistan suture zone (Camp and Griffis 1982), Zabol–Baluch zone (Berberian and King 1981), flysch zone (Eftekharnejad 1981), Makran mountain, and East of Iran (Stöcklin 1968). Sistan suture zone has tectonically changed by many events during a short geological time (Camp and Griffis 1982). A rifting system has parted Lut and Afghan blocks from each other. Afterwards an oceanic basin appeared that its evidence is thick flysch deposits. Northeastward subduction zone into the Afghan block occurred in Maastrichtian and collision of Lut block and Neh complex happened in Eocene. Continuing of the convergence caused the folds and conjugate strike slip faults that are visible on Oligocene and Miocene rocks (Camp and Griffis 1982). The subduction has been to the east direction where Afghan block exists (Tirrul et al. 1983). However, the number of Afghanistan volcanoes is trifle. Taftan volcano is a young and semi-active Pliocene-quaternary volcanic that is located in 50 km far from Khash village in Baluchistan (Gansser 1966). Its height from the sea level is 4050 m and from surrounding planes is about 2000 m. This volcano has occurred on Eocene flyschs. The first eruptions involve lava, dacite, and rhyodacite pyroclastic rocks. The second activity of Taftan volcano consist upper Pliocene dacite and andesite lava with widespread agglomerate layers in 10 km far from its cone.

It is believed that Taftan volcano is due to the subduction of Arabian plate into the central Iran plate. According to the geodynamics models about closing of Neotethys Ocean, this subduction has some important seismic evidences (Ambraseys and Melville 1982). SF is a reverse seismogenic fault with a right lateral component in its latest movements. The study area involves also Oligocene granodiorite intrusive body called Kuh-e-Sefid Mountain and metadacite body called Kuh-e-Gazu Mountain. Both of them are located in east of Taftan volcano and SF. To simplify geological units and have dominance to the area, we provide a geological simplified map (Fig. 1) based on geological setting map from the area (Eftekharnezhad et al. 1987). According to the map, two main mentioned igneous bodies have a northwestward thinning. The slender morphs show an obvious synchronization with SF curvature (Fig. 2a).

Lithological sequence

To have an overall view of the lithological sequence in the study area, we provide a general geological map by simplifying lithological units (Fig. 1). Although the main study area, including SF lies in eastern side of Taftan volcano (Fig. 2b) it spreads to the western side of Taftan volcano including Nosratabad and Bamposht faults. However, we mainly focus on eastern area of Taftan volcano to get analytical data from SF and nearby igneous rocks. We also consider general structural data from the western region to provide an overall model as discussed in the following. Cretaceous colored melange outcrops are oldest units in the study area (Fig. 1). In general, flysch facies developed in Eocene. Metadacites and intrusive granodiorites called Kuh-e-Sefid developed in Paleo-Eocene and Eo-Oligocene respectively (Fig. 1).

Main faults and related fractures

The main stations of attitude measurements for faults and fractures are around strike of SF. In order to obtain after-Eocene related stress fields and to provide a model based on these stress fields, all the stations are selections with respect to their geological time. The stations of fractures are around some villages called Sangan, Pilkushkan, Sabzgaz, Hasanabad, Ladiz, Rankazan, and Bayan. Attitude of fracture sets from these stations are drawn in the stereograms (Fig. 3). Moreover, In coordination 28°15′N, 61°43′E the Limestone unit shows obvious tension gashes that confirm dextral movements in this region (Fig. 4). The after-Eocene related orientations of the fault planes of the study area are referred as dihedral calculations and Rose diagrams (Fig. 5).

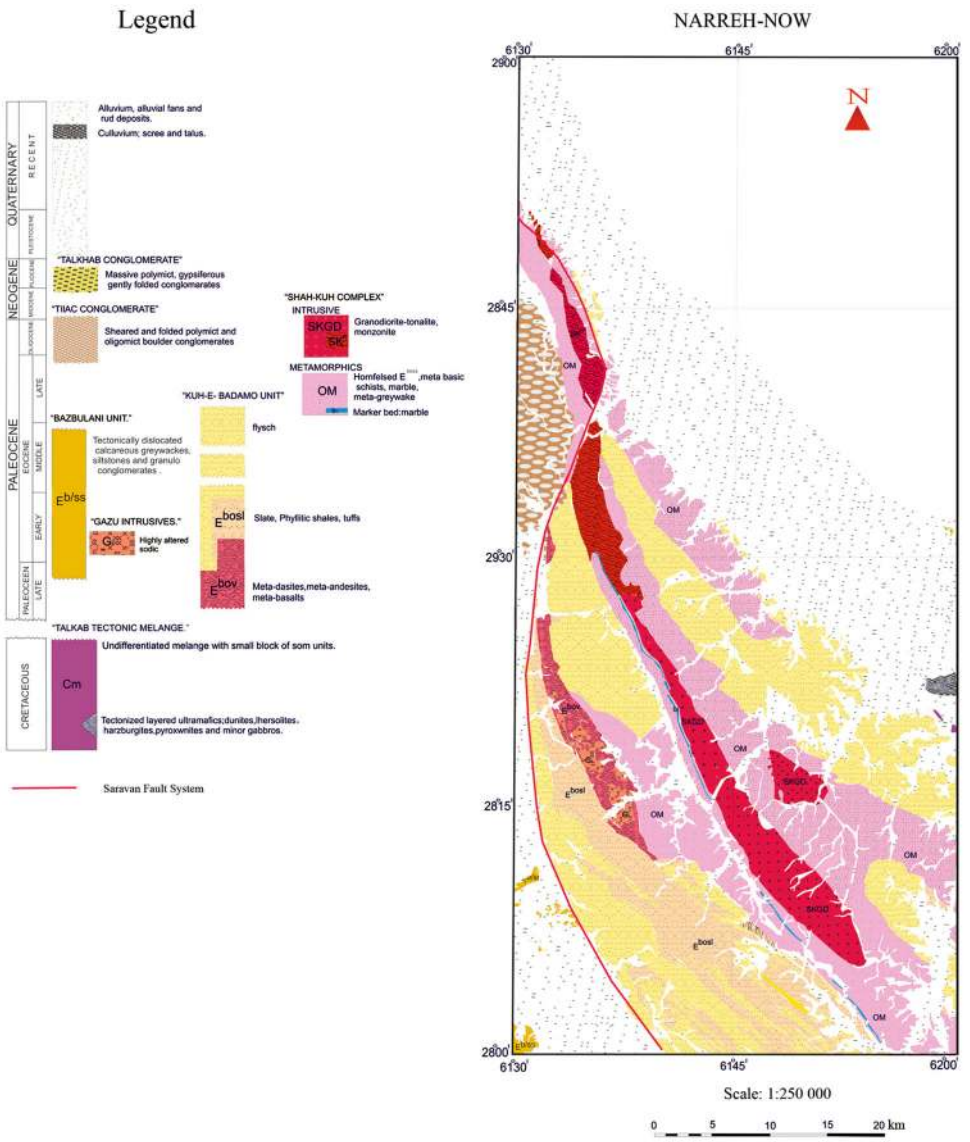

Fig. 1 Simplified geological setting map for study area. As seen, two main igneous units that marked as SKGD and E^{bov} have more pinch outing toward northwest direction

Strain and stress analysis

Calculating strain ratio along SF

Strain ratio calculation from features through accessible angular changes is common (Ragan 2009; Fossen 2010). Along N28W striking as main strike of SF, linear structures such as folds axis show synchronization in their trend with the moment variations of the fault strike (Sadeghi and Moridi 2009a, 2009b). The assumption is that the change of the main trend of SE is a sign of deformation in the study area. Therefore, we consider the lines parallel to the main trend of SE as passive markers and tangent lines as active markers at the selected stations. The curvature of SF clearly starts at 28°8′N, 61°34′E (Fig. 2). The basis of strain ratio calculation is the construction methods using Mohr's circle for strain. By having two deformed structures, it is possible to measure the shear deformation angle $\psi 1$ and $\psi 2$ (Ramsay 1967; Ramsay and Huber 1983). By getting ψ from different stations and drawing tangent lines to the original curve that are derivative of fault function in a certain coordination, it is possible to calculate strain ratio through finite strain Mohr's circle and to find reciprocal quadratic elongation from following equation,

$$R_s = \sqrt{\lambda_2'/\lambda_1'} \quad (1)$$

where R_s is strain ratio and λ' is reciprocal quadratic elongation. Different stations on SF are candidate for strain ratio calculations (Fig. 6). The most value is 7.40 for stations 5 and 6 that just lie on the location with most curvature of fault strike (Fig. 6).

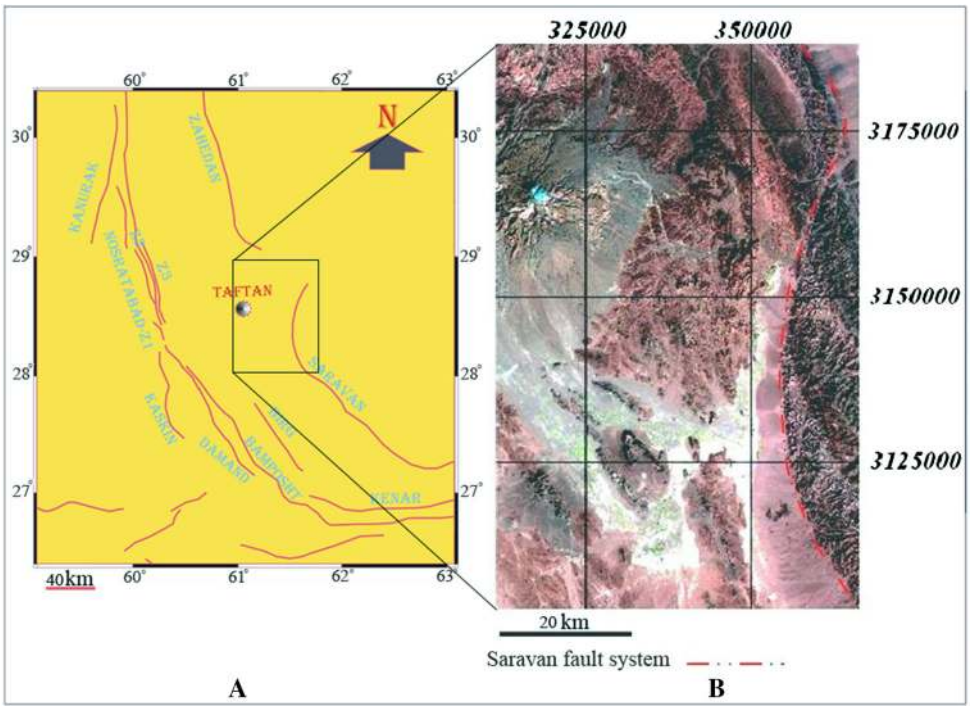

Fig. 2 **a** Graphical layout of main faults around the study area. **b** Landsat (TM) image from study area in the east of Taftan volcano and curvature of Saravan fault

Calculating stress field

Although simultaneous stress field studies led to insight into the mechanics that drives plate motions (e.g. Dwivedi and Hayashi 2010) but deductions will be difficult when studies encompass a more time range. A 2-D stress distribution is possible to consider in two states. The first state includes a horizontal plane with two dimensions and the other one includes a plane with two horizontal and vertical planes (e.g. Islam and Shinjo 2012). Estimating of stress distribution is commonly from major to regional scale (Zhang et al. 2011). Nevertheless, according to conception of finite element analyses, we gather local data and generalize collected data to the whole area.

There are different types of faults and fractures in eastern region of Taftan volcano. Finding out the type of fault and fractures is possible through different ways. Besides, some folds and fractures related to the main faulting system can help us to infer special direction of maximum horizontal principal stress, S_{Hmax} (Sadeghi and Moridi 2009a, 2009b). For example when there is a plenty of conjugate fractures around fault zone that overlap other younger structures, it is possible to estimate latest direction of S_{Hmax}. In the other hand, the dip of local fault planes and displacement vectors are useful for stress analysis. Four stations are important for considering along main strike of SF. The stations include those are located from the south to the north on the main strike of the fault first curvature, inflection point, and second curvature (Fig. 7). Therefore, we can estimate the stress ratio using analytical method based on Mohr's circle (Fig. 7). The Basis for this aim is NDA (numerical-dynamic analysis) method (Spang 1972). It is noticeable that the plots represents a dimensionless Mohr's circle of the plane $\sigma_1 - \sigma_3$. Therefore, the absolute values of σ_1 and σ_3 is not important but the situation between σ_1 and σ_3, where two small circles come together is valuable to estimate stress ratio. To provide stress field in eastern Taftan volcano, a MATLAB programming is applied. The programming focuses on plane stress analysis. By assuming a linear elastic material, we obtain stresses as

$$\sigma = \begin{bmatrix} \sigma_x \\ \sigma_y \\ \sigma_z \end{bmatrix} = \begin{bmatrix} \frac{E}{1-v^2} & \frac{vE}{1-v^2} & 0 \\ \frac{vE}{1-v^2} & \frac{E}{1-v^2} & 0 \\ 0 & 0 & G = \frac{vE}{1-v^2} \end{bmatrix} \begin{bmatrix} \varepsilon_x \\ \varepsilon_y \\ \gamma_{xy} \end{bmatrix} \quad (2)$$

where E is the modulus of elasticity and v is the Poisson's coefficient. ε is strain and γ is transverse shear. The static equilibrium equations are defined as

$$\frac{\partial \sigma_x}{\partial x} + \frac{\partial \tau_{xy}}{\partial y} + b_x = 0 \quad (3)$$

$$\frac{\partial \tau_{xy}}{\partial x} + \frac{\partial \sigma_y}{\partial y} + b_y = 0 \quad (4)$$

where b_x, b_y are body forces.

The values of stress ratio on SF are as controller points. To draw more accurate stress field, measuring orientation

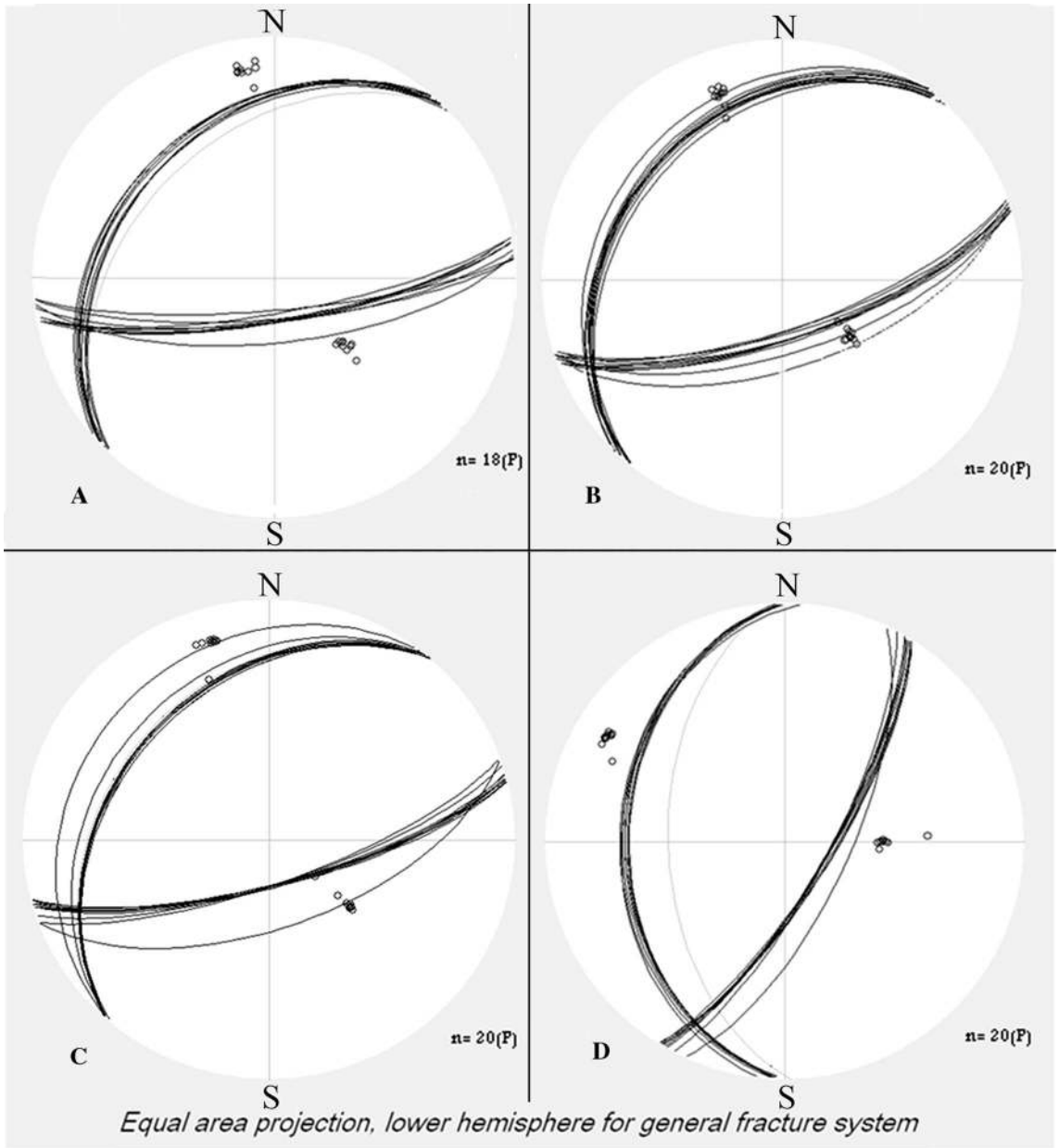

Fig. 3 Stereograms of conjugate fractures orientation including arcs and poles for the stations **a** eastern mountains of Sangan, **b** Ladiz and Rankazan, **c** Pilkushkan, and **d** Bayan

of structures in across eastern region of Taftan volcano is necessary. We divide the research area into smaller areas and estimate directing of main stress vectors related to conjugated fractures about a same geological time in each area. By collecting vector data and relative numerical results of stress ratio, it is possible to provide a stress field by running MATLAB coding (Fig. 8). This field is separable into two groups for study. Group 1 is located around east and northeast and partially southeast of Taftan volcano that obviously follows the unit stress source. Group 2 is located around the southeast of Taftan and has less signs of irregularities. The second group has a source other than Taftan volcano. However, there is a significant compatibility between attitude of structures and stress field net, but a conflict exists between related attitudes in the group 1 and 2.

By passing from the first group to the second one, the conflict becomes less and structures become more compatible with the stress field. Also in the group 1, it seems that stress field is in relation to a volumetric strain due to Taftan volcano. Thus, the volumetric strain in the first group must be taken seriously. Therefore, superposition of

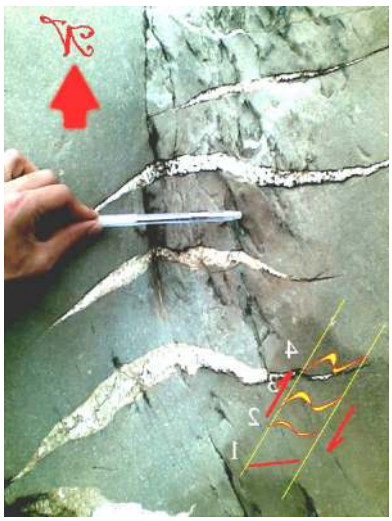

Fig. 4 Tension gashes around right lateral shear zone in Oligo-Miocene sandstone unites that marked as OMm (Fig. 1)

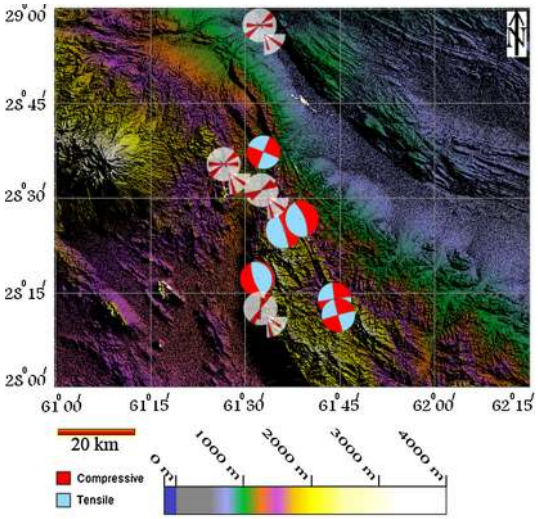

Fig. 5 Dihedral calculations and rose diagrams of fault planes orientation plotted on the overall DEM map at study stations on eastern Taftan. All study stations are in relation to the after-Eocene formations

stress systems led to the greater complexity in this area. Conceptions of superposition suggest additivity property of two or more vectors (Spiegel 1959; Ragan 2009) in many physical issues. The equation expressing additivity property of two stress matrices is

$$A + B = C \tag{5}$$

This means when two stress fields affect simultaneously, the size and orientation of the effective stress is different from when each stress field affects separately. For example, if we have two groups of stress fields affecting in a region, we must have a combination of stress field as a resultant. Mathematically, when each stress field is unit matrix, the resultant matrix will be unit.

$$\begin{bmatrix} \sigma x_1 & \tau xy_1 & \tau xz_1 \\ \tau yx_1 & \sigma y_1 & \tau yz_1 \\ \tau zx_1 & \tau zy_1 & \sigma z_1 \end{bmatrix} + \begin{bmatrix} \sigma x_2 & \tau xy_2 & \tau xz_2 \\ \tau yx_2 & \sigma y_2 & \tau yz_2 \\ \tau zx_2 & \tau zy_2 & \sigma z_2 \end{bmatrix} = \begin{bmatrix} \sigma x_1 + \sigma x_2 & \tau xy_1 + \tau xy_2 & \tau xz_1 + \tau xz_2 \\ \tau yx_1 + \tau yx_2 & \sigma x_1 + \sigma y_2 & \tau yz_1 + \tau yz_2 \\ \tau zx_1 + \tau zx_2 & \tau zy_1 + \tau zy_2 & \sigma z_1 + \sigma z_2 \end{bmatrix} \tag{6}$$

S_{Hmax} for group 1 is a resultant of two stress regimes: first, affected stress before volumetric strain according to the group 2; second, the stress due to volumetric strain. Therefore, we identify the group 1 as a resultant stress field. By using stress field and tectonic data, we provide a portrayal of general structures for the S_{Hmax} (Fig. 9).

Three-dimension mechanical model

Primary mechanical model

By having the basic information from research area, we try to provide a 3D view of occurred mechanisms. From morphologically viewpoint, the overall shape of a model is due to the most important reasons. Therefore, existence of a comparative default is necessary and helps to have understanding of problem. One of ways to get defaults is considering analogue models. Based on sandbox experiments (Dominguez et al. 1998; Marques and Cobbold 2002; Zweigel 1998) there should be an indenter as rigid mass within a compression zone to have curved morphology like the study area. However, there are some difference between morphology of study area and finite morphology due to sandbox models. The most important of them is width of structural band that is greater than our research area. The other difference is a curved discontinues band in comparison with continues SF (Fig. 10). Therefore, we need a more detailed primary model to understand the occurred mechanism. By designing a simple mechanical model in Ansys, we show a bulking between two planes that affect to the strike of SF and make curvatures. In this primary model, a set of parallel thin sheets of copper lie in a fluid-filled chamber. Fluid is defined with special characters as Reference Density equal to 998 kg/m^3 and Reference Bulk modulus equal to 2.2e + 90 Pa. An elastic air bag among planes of copper sheets is gradually filled with air. Selecting of Copper is because of its rather moderate Young's modulus equal to 117 GPa, high ductility, and flexibility properties. In the changes of the deformation path, copper has low intensive influence (Niewielski and Kuc 2009). This helps us to control extra deformations and have an ideal deformation. According to earned strain ratio (Fig. 6) and difference of average Young's Modulus

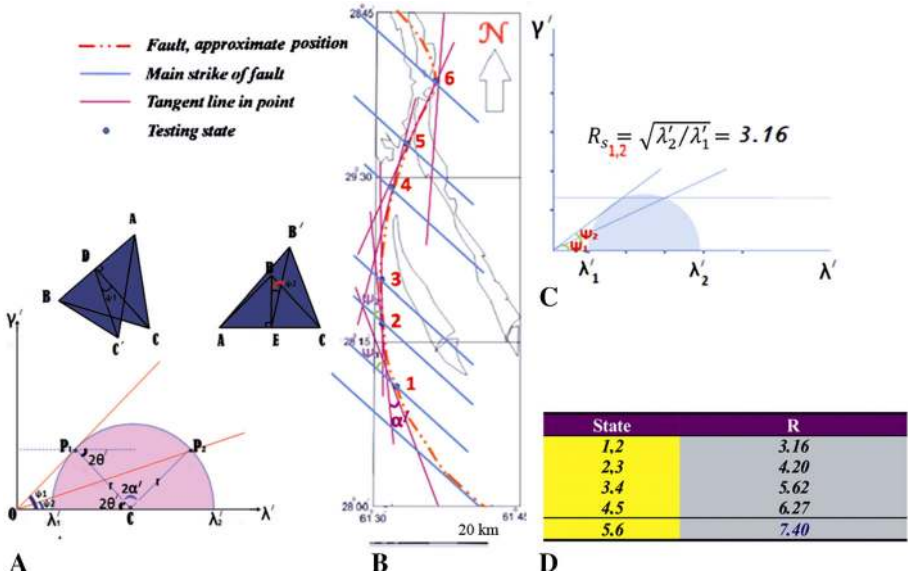

State	R
1,2	3.16
2,3	4.20
3,4	5.62
4,5	6.27
5,6	7.40

Fig. 6 Calculating strain ratio in Saravan fault. **a** Overall method **b** Graphical layout of Saravan fault shows main markers. As seen, for each station there are two lines including line of main strike of fault (*blue*) and tangent line of fault (*pink*). With generalization method for lines deviation from main strike, we can obtain the relative values of strain ratio. **c** An example solution for stations 1 and 2. Note that for each two stations, drawing of related Mohr's circle is necessary. **d** Calculated values for all six stations

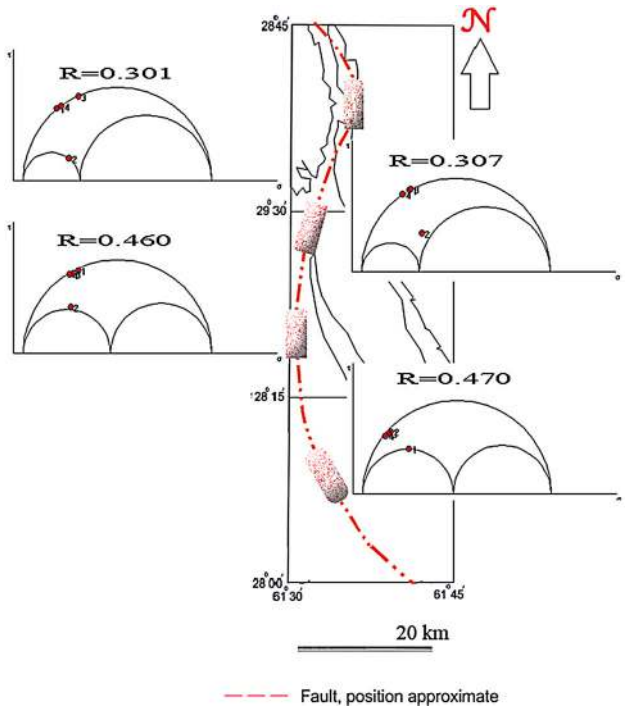

Fig. 7 The response of numerical-dynamic analysis after Spang (1972) on the Mohr's circles (see text)

between rock samples in Table 1 and copper, the simulation continues to the strain limit equal to 11. After filling the air bag, deformed planes show typical curvature (Fig. 11) that suggest an overall likeness with deformation pattern in the study region. At this step, we realize that a rigid mass and bulking can play role in deforming. This event is just a superficial likeness that gives us a primary view of the depth of the ground and is assigned to the

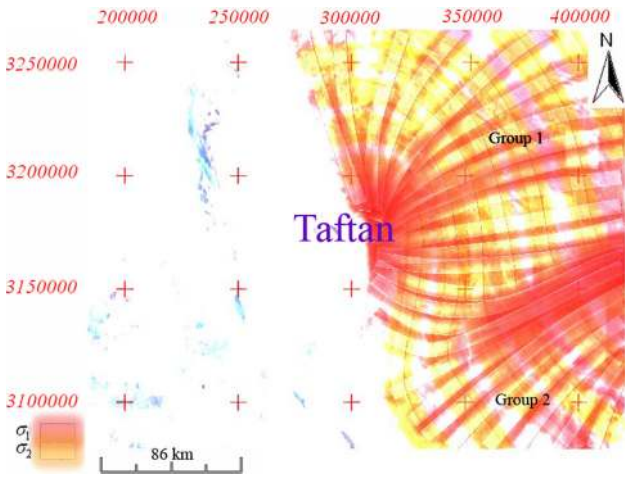

Fig. 8 General stress field map for eastern region of Taftan volcano. As seen, two groups of subfields are detectable. The map is due to coding 2-D stress equations in MATLAB (see text)

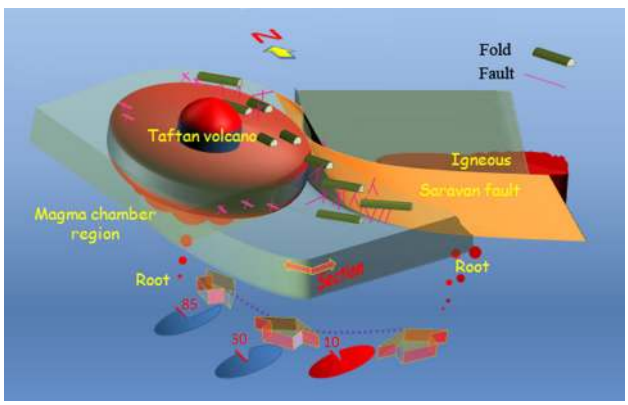

Fig. 9 The portrayal represents rotation range of S_{Hmax} orientation for related structures from Eocene until Oligo-Miocene

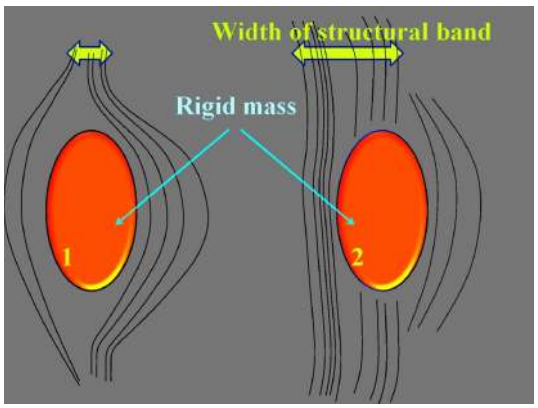

Fig. 10 A structural comparison between research area (with rigid mass *1*) and sandbox models (with rigid mass *2*). Note to the differences of width of structural band along the large diameters of ellipses and continuity of curved bands between *1* and *2*

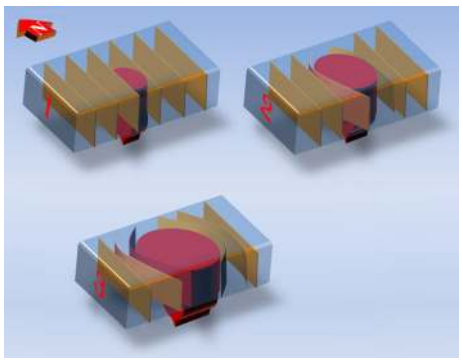

Fig. 11 A primary mechanical model for bulking. The curvature of the parallel copper sheets increases from stages 1 to 3 with increasing the volume of elastic air bag

magma chamber evolutions or something else similar that needs more works.

Combined mechanical model

By having primary mechanical insight from previous section, we complete the model by affecting general stress field to the bulking model (Fig. 11). In this way, besides of bulking due to the volumetric strain and its related stress field, the model includes another stress field with different magnitude and orientation. This field is due to the plate tectonics forces that here is because of Makran subduction zone (Rollinson et al. 2014) and Miocene Arabia-Eurasia collision (Okay et al. 2010) as a compression mechanism with certain direction of maximum stress. Combining two gained models give an integrated model. Due to the same forces of governing compression mechanism in over time, the resultant after-bulking mechanism has a different nature than the previous mechanism that explain attitude of the structural elements in the research study area specially in group 1 (Fig. 12).

Simulation

Since SF plane is the main curved structure and extrusive bodies follow its curvature, we import all curvature length and its related structural data into the model. For this aim, we use a collection of software such as Surfer, AutoCAD, GOCAD, Ansys, and some mediator applications. To create each structure such as igneous bodies, we need to the control points. These points include databases of 3D coordination. They are convertible to the matrices after processing (Martin 1966; Przemieniecki 1968; Golub and Van Loan 1996) and are readable for analytical software such as Ansys. The design method follows the steps of creating points, creating lines by points, and creating surfaces through lines. In this way, a surface is a result of expanding a line along another line. Therefore, to create a fault plane, one line is parallel to strike and the other one is parallel to dip direction. From now on, we apply the rock mechanical data from different stations in Table 1 to the model. Besides, we affect the stress directions (Fig. 12) and stress field of study area to the SF as a solid part. We consider the plane of SF as a flat surface and mesh it through structured meshing method about linear structures (Reddy 1993; Hughes 2000; Cook et al. 2002; Zienkiewicz et al. 2005; Bathe 2007). It is noticeable that in this simulation fault plane is a thin part of hanging wall block. In fact, we determine boundary condition for the blocks. In our finite element problem, calculation steps typically are:

- Definition a set of elements connected at nodes
- Computation of stiffness matrix $K^{(e)}$ and force vector $F^{(e)}$ for each element
- Assembling the contribution of all elements into the global system $Ka = f$
- Modifying the global system by imposing essential (displacements) boundary conditions
- Solving the global system and obtaining the global displacements a

Taking into account the boundary conditions $u_1 = u_2 = u_3 = 0$, we may write

$$\begin{bmatrix} K_1 & -K_1 & 0 & 0 \\ -K_1K_1 & +K_2+K_3 & -K_2 & -K_3 \\ 0 & -K_2 & K_2 & 0 \\ 0 & K_3 & 0 & -K_3 \end{bmatrix} \begin{Bmatrix} 0 \\ u_3 \\ 0 \\ 0 \end{Bmatrix} = \begin{Bmatrix} F_1 \\ P \\ F_3 \\ F_4 \end{Bmatrix} \tag{7}$$

Therefore, it is possible to compute the reactions F_1, F_3, F_4 after the computation of the global displacements.

The analyzing of such features has a shell-based approach (Adini 1961). To focus on faults plane and have a

Table 1 Rock mechanic data collected from different locations

Location latitude longitude	Rock type	Relative density (ASTM C97) g/cm^3	Uniaxial compressive strength (ASTM C170) MPa	Point load strength MPa	Young's modulus $\times 10^3$ MPa
N: 28°15′ E: 61°44′	Granodiorite	2.67	175.3	12.1	60.2
N: 28°20′ E: 61°41′	Granodiorite	2.64	174.2	11.9	59.8
N: 28°11′ E: 61°46′	Diorite	2.84	204.1	14.3	77.3
N: 28°17′ E: 61°43′	Tonalite	2.74	190.4	13.2	65.1
N: 28°13′ E: 61°45′	Tonalite	2.75	191.1	13.4	66.2
N: 28°15′ E: 61°37′	Metadacite	2.71	193.5	13.1	65.7
N: 28°28′ E: 61°32′	Metadacite	2.67	192.9	12.9	65.4
N: 29°34′ E: 61°34′	Gneiss	2.68	163.4	12.8	45.5
N: 28°15′ E: 61°33′	Schist	2.65	82.4	6.1	35.3

Samples are analyzed in Rock Mechanics Laboratory at University of Tabriz

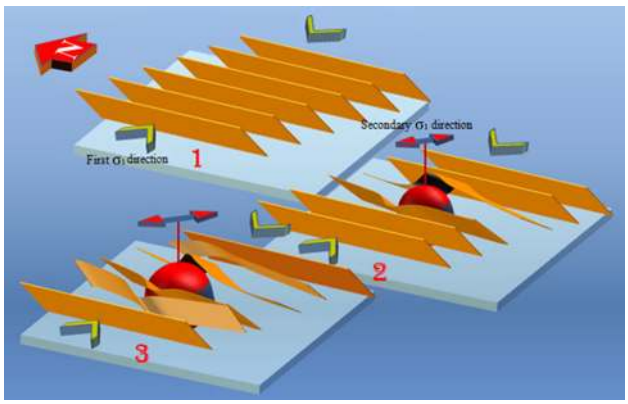

Fig. 12 A mechanical model for representing the stress evolutions in the research area. Happening of a compression and then volumetric strain in the stages *1* and *2* respectively and continuing from stage *3* simultaneously

better view of deformation, we ignore block mass except a thin thickness across the fault plane. Therefore, we select SF before its curvature in length about 240 km, with its hanging wall block. After defining the control points on the fault plane and hanging wall block, we mesh them (Fig. 13) based on a node distance of 24 km. We subject the faults surface as a narrow part of the hanging wall block to the discussed mechanisms (i.e., Fig. 12) and define stress fields. For bulking, an asunder zone affects the faults strikes. After several running and correcting to reach reasonable response (Fig. 14), the final geometry of the fault plane appears (Fig. 15). By revealing the fault plane, it can be seen a right lateral progressing tear zone at the south end of the fault beneath the igneous bodies. Its growth direction from its tip point is upward to the northwest direction

Conclusions

3D model of the SF plane based on stress field and mechanical simulated models suggests the combined stress field effects as an important item that influence fault plane. It also show the mechanical behavior of the fault plane could vary from surface to the depth in different stress fields. Two gained main groups of stress fields represent S_{Hmax} orientation range from N10E to N85E. Comparing results of analogue models (i.e. Dominguez et al. 1998; Marques and Cobbold 2002; Zweigel 1998) and our primary models suggests for existence of a compression in the beginning until Eocene, a volumetric strain in Oligo-Miocene, and continuing of both simultaneously. Existence of a tear zone (Fig. 12) at the south end of the fault maybe justifies normal focal mechanism of Saravan earthquake on 16 April 2013. In conclusions, while other items may contribute to the geometry of fault plane, the most important finding in our model is effects of resultant stress

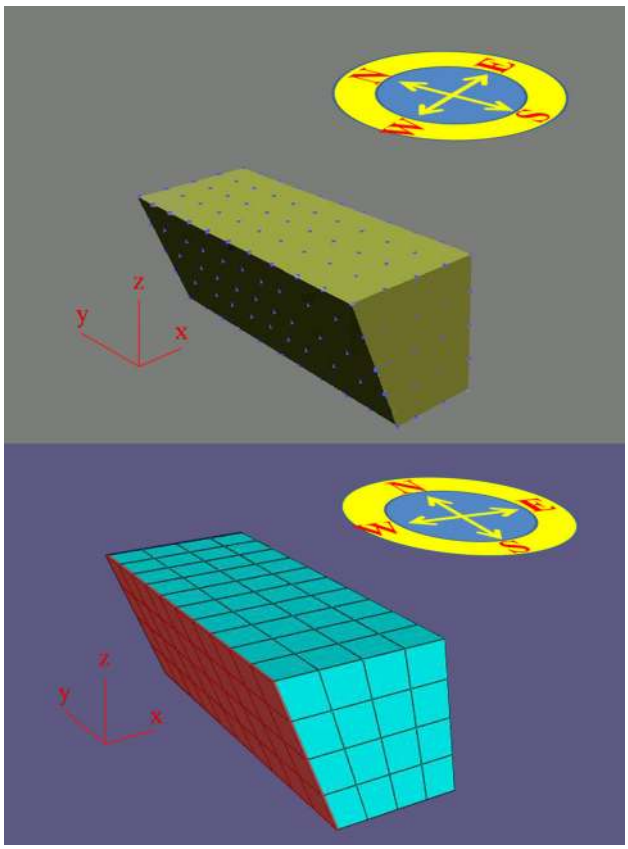

Fig. 13 Saravan fault plane with its hanging wall block. (*Above*) Definition control points by interpolation of the intersection of parts lines on the fault plane and whole of block with distance of 24 km between each point in x, y, and z direction. (*Below*) Structured meshing for whole of block with distance of 24 km between each node in y and z direction. Fault plane is distinct as the *red* part

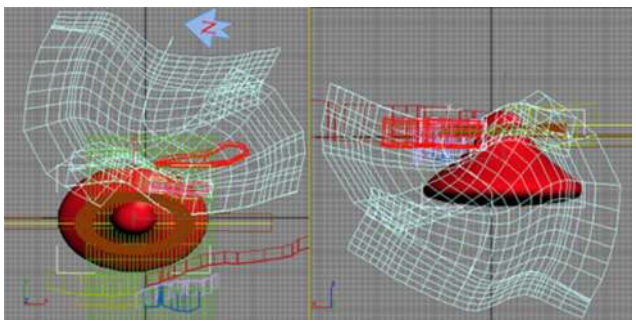

Fig. 14 Deformed elements of Saravan fault surface as *white colored net* after applying bulking and compression mechanic. (*Left*) View from top and (*Right*) east of the study area. The elements of igneous masses (*red*) and other faults system in western region of the study area (in different colors) are also shown. It can be detected the progressing tear zone at the south end of the fault (see text)

fields in inhomogeneous deformations of faults planes. However, the more accurate information about underground fault mechanisms needs more works. We have not

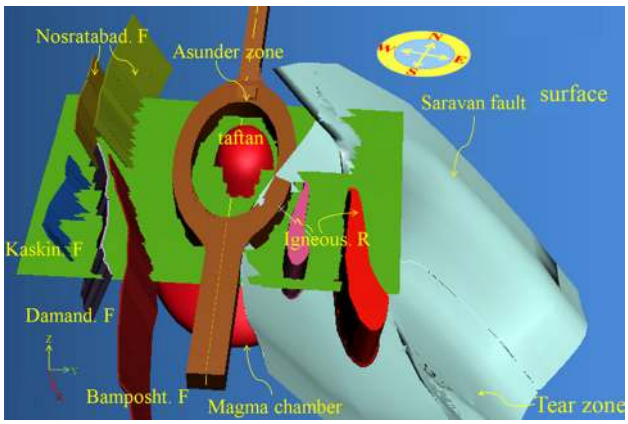

Fig. 15 Final geometry of fault surface subjected to the affecting compression and bulking. Tear zone is progressing upward in NW direction

considered accurate displacement vectors in this model. Affecting a more range of kinematic data to determine boundary conditions that are more accurate is one of the future objects.

Acknowledgments We thank E. Gholami from University of Birjand who shared his information and knowledge about SF and general geology. Analysis of the rock mechanic data to support this article in Table 1 has performed by us in the Rock Mechanics Laboratory at University of Tabriz and has not published anywhere else. We also thank officials at University of Tabriz and laboratory expert M. Sharghi for cooperation.

References

Adini A (1961) Analysis of shell structures by the finite element method. Dissertation, University of California

Alavi M (1991) Tectonic map of the Middle East (1:2900000). Geo. Surv. Iran

Ambraseys N, Melville C (1982) A history of Persian earthquakes. Cambridge University Press, Cambridge

Bathe KJ (2007) Finite element procedure. Prentice-Hall, London

Beaumont C, Ellis S, Hamilton J, Fullsack P (1996) Mechanical model for subduction-collision tectonics of alpine-type compressional orogens. Geology 24:675–678

Berberian M, King G (1981) Towards a paleogeography and tectonic evolution of Iran. Can J Earth Sci 18:210–265

Byrne DE, Wang W, Davis M (1993) Mechanical role of backstops in the growth of forearcs. Tectonics 12(1):123–144

Camp V, Griffis R (1982) Character, genesis, and tectonic setting of igneous rocks in the Sistan suture zone, eastern Iran. Lithos 15:221–239

Carlson J, Langer MJS (1989) Mechanical model of an earthquake fault. Am Phys Soc 40:6470–6484

Chéry J, Zoback MD, Hassani R (2001) An integrated mechanical model of the San Andreas fault in central and northern California. J Geophys Res 106(B10):22051–22066

Chéry J, Zoback MD, Hickman S (2004) A mechanical model of the San Andreas fault and SAFOD pilot hole stress measurements. Geophys Res Lett 31:1–5

Chinnery MA (1961) The deformation of the ground around surface faults. Bull Seismol Soc Am 51:355–372
Chinnery MA (1970) Earthquake displacement fields. In: Mansinha L (ed) Earthquake displacement fields and the rotation of the earth. Springer, New York, pp 17–38
Cook RD, Malkus DS, Plesha ME, Witt RJ (2002) Concepts and applications of finite Element analysis, 4th edn. Wiley, New York
Dominguez S, Lallemand SE, Malavieille J, Von Huene R (1998) Upper plate deformation associated with seamount subduction. Tectonophysics 293:207–224
Dwivedi SK, Hayashi D (2010) Modeling the contemporary stress field and deformation pattern of eastern Mediterranean. J Earth Sci 21:365–381
Eftekharnejad J (1981) Tectonic division of Iran with respect to sedimentary basins. J Iran Pet Soc 82:19–28 **(in Farsi)**
Eftekharnezhad J, Lioyd B, Squire A, Odinga M, McCormic C, Griffiths P (1987) Geological map of Nareh-Now quadrangle, Scale 1:250000, No. M-12, GSI
Fossen H (2010) Structural geology. Cambridge University Press, Cambridge
Gansser A (1966) The Taftan volcano (SE Iran). Eclogae Geol Helv 64:319–344
Golub GH, Van Loan CF (1996) Matrix computations, 3rd edn. Johns Hopkins University Press, Baltimore
Hughes TJR (2000) The finite element method. Dover Publications, New York
Islam MS, Shinjo R (2012) The Dauki Fault at the Shillong Plateau-Bengal basin boundary in northeastern India: 2D finite element modeling. J Earth Sci 23:854–863
Marques FO, Cobbold PR (2002) Topography as a major factor in the development of thrust belts: insights from sandbox experiments. Tectonophysics 384:247–268
Martin HC (1966) Introduction to matrix methods of structural analysis. McGraw-Hill, New York
Nabavi MH (1976) An introduction to the Iranian geology. Geological survey of Iran, Report No. 38, pp: 110, (In Farsi)
Niewielski G, Kuc D (2009) Structure of the copper under controlled deformation path conditions. J Achiev Mater Manuf Eng 36:20–27
Niño F, Chéry J, Gratier JP (1998) Mechanical modeling of compressional basins: origin and interaction of faults, erosion, and subsidence in the Ventura basin, California. Tectonics 17(6):955–972
Nur A, Mavko GM (1974) Postseismic viscoelastic rebound. Science 183:204–206
Okay AI, Zattin M, Cavazza W (2010) Apatite fission-track data for the miocene Arabia-Eurasia collision. Geology 38:35–38
Przemieniecki JS (1968) Theory of matrix structural analysis. McGraw-Hill, New York
Ragan DM (2009) Structural geology: an introduction to geometrical techniques. Cambridge University Press, Cambridge
Ramsay JG (1967) Folding and fracturing of rocks. McGraw-Hill, New York
Ramsay JG, Huber MI (1983) The techniques of modern structural geology, vol 1: strain analysis. Academic Press, London
Reddy JN (1993) An introduction to the finite element method, 2nd edn. McGraw-Hill, New York
Rhoden AR, Wurman G, Huff EM, Manga M, Hurford TA (2012) Shell tectonics: a mechanical model for strike-slip displacement on Europa. Icarus 218:297–307
Rollinson HR, Searle MP, Abbasi IA, Al-Lazki AI, Al-Kindi MH (2014) Tectonic evolution of the Oman mountains: an introduction. Geol Soc Lond 392:1–7
Rowshandel B, Nemat-Nasser S (1986) A mechanical model for deformation and earthquakes on strike-slip faults. PAGEOPH 124(3):533–566
Rybicki K (1971) The elastic residual field of a very long strike-slip fault in the presence of discontinuity. Bull Seismol Soc Am 61:79–92
Sadeghi P, Moridi AA (2009) Strain rate calculation in eastern region granodiorites of Taftan volcano near to the Kuhrud fault. The seventh Iranian students' conference of mining engineering. Tabriz, Sahand University of Technology Press 429–434 (in Farsi)
Sadeghi P, Moridi AA (2009) Calculation of stress and strain rate in linear structural elements around eastern Taftan volcano. The 3rd symposium of geology of Payame noor University. Isfahan. Isfahan Payame Noor University Press 199–202 (in Farsi)
Spang J (1972) Numerical method for dynamic analysis of calcite twin lamellae. Geol Soc Am Bull 84:134–150
Spiegel MR (1959) Schaum's outline of theory and problems of vector analysis and an introduction to tensor analysis. Schaum, New York
Steketee JA (1958) Some geophysical applications of the elasticity theory of dislocations. Can J Phys 36:1168–1198
Stöcklin J (1968) Structural history and tectonics of Iran: a review. Am Assoc Pet Geol Bull 15:1229–1258
Stuart WD (1979) Strain softening prior to two-dimensional strike-slip earthquakes. J Geophys Res 84:1063–1070
Stuart WD (1981) Stiffness method for anticipating earthquakes. Bull Seismol Soc Am 71:363–370
Stuart WD, Mavko GM (1979) Earthquake instability on a strike-slip fault. J Geophys Res 84:2153–2160
Tirrul R, Bell L, Griffis R (1983) The Sistan suture zone of eastern Iran. Geol Soc Am Bull 84:134–150
Weertman J (1965) Relationship between displacements on a free surface and the stress on a fault. Bull Seismol Soc Am 55:945–953
Willet S, Beaumont C, Fullsack P (1993) Mechanical model for the tectonics of double vergent compressional region. Geology 21:371–374
Zare M, Shahvar M (2013) An urgent report on the Saravan, Iran earthquake of 16 April 2013 Mw7.7, a quick engineering seismological overview. Rep, IIEES, Tehran, Iran
Zhang S, Xing HL, Yuen DA, Zhang HA, Shi YL (2011) Regional stress fields under Tibet from 3D global flow simulation. J Earth Sci China 22(2):155–159
Zienkiewicz OC, Taylor RL, Zhu JZ (2005) The finite element method, 6th edn. Elsevier, New York
Zweigel P (1998) Arcuate accretionary wedge formation at convex plate margin corners: results of sandbox analogue experiments. J Struct Geol 20(12):1597–1609